International Journal of Greenhouse Gas Control 75 (2018) 98–106

Contents lists available at ScienceDirect

International Journal of Greenhouse Gas Control

journal homepage: www.elsevier.com/locate/ijggc

Performance of a 50 kW_{th} coal-fuelled chemical looping combustor

Jinchen Ma, Xin Tian, Chaoquan Wang, Xi Chen, Haibo Zhao*

State Key Laboratory of Coal Combustion, School of Energy and Power Engineering, Huazhong University of Science and Technology, Wuhan, 430074, PR China

ARTICLE INFO

Keyword:
Chemical looping
Reactor
Coal
Operation

ABSTRACT

A 50 kW_{th} chemical looping combustion (CLC) reactor for coal has been successfully constructed and operated. A turbulent fluidized bed acts as the air reactor (AR) to achieve high solid circulation rate, while a bubbling fluidized bed operates as the fuel reactor (FR) to guarantee sufficient solid residence time. Two risers are separately connected to the AR and FR to provide the driving force for oxygen carrier (OC) circulation. A four-chamber loop seal (LS) is installed between AR and FR, playing the roles of a gas-sealing configuration and also a carbon stripper to convert unreacted char.

Low-cost natural hematite was used as OC and Shenhua bituminous coal was used as fuel. A series of tests was conducted to investigate the performance of the newly constructed CLC reactor under different operational parameters. Effects of temperature, inlet gas velocity and H_2O concentration in fluidizing agent, on the performance of the CLC reactor were investigated. The relatively stable pressure drop attained in the FR indicated successful operation of the CLC system. During 120 min continuous running with a bed inventory of 100 kg in FR, the highest CO_2 yield reached to 0.91 and the combustion efficiency was 0.86 at 1000 °C.

1. Introduction

With the global concerns over climate change, the development of carbon capture and storage (CCS) technologies for CO_2 mitigation is of urgent need (Chevallier, 2010). Chemical looping combustion (CLC), with the characteristic of inherent CO_2 separation, is regarded as one of the most promising ways to capture CO_2 (Ishida and Jin, 1994). In a typical CLC process, oxygen carrier (OC), usually a kind of metal oxide being supported by inert materials, circulates between the air reactor (AR) and fuel reactor (FR) to transfer lattice oxygen needed for fuel conversion. In this way, the traditional one-step combustion process is split into two separate steps, as Eqs. (R1) and (R2) in FR and AR, respectively. In this way, direct contact between air and fuel is avoided. Consequently, high-purity CO_2 can be obtained after steam condensing from the exhaust of FR. By far, interconnected fluidized bed, which was first proposed by Lyngfelt et al. (2001), has been demonstrated as the most suitable reactor system for the implementation of CLC processes.

$$(2n + m/2)\mathrm{MeO} + C_nH_m \rightarrow n\mathrm{CO_2} + m/2\mathrm{H_2O} + (2n + m/2)\mathrm{Me} \quad \text{(R1)}$$

$$\mathrm{Me} + 1/2\mathrm{O_2} \rightarrow \mathrm{MeO} \quad \text{(R2)}$$

For the development of CLC technology, the research work was mainly on OC screening and optimization, gas-solid reaction kinetics between OC and fuel gas, as well as reactor design and operation during the past few decades (Adanez et al., 2012; Mattisson, 2013). OCs with different active compounds and inert supports have been applied to different types of chemical looping processes. Fe-, Ni-based OCs were usually adopted in CLC with gaseous/solid fuels by transporting lattice oxygen (Bao et al., 2013b; Leion et al., 2008; Shen et al., 2009). Cu-, Mn- and Co-based OCs were used for chemical looping with oxygen uncoupling (CLOU) by releasing gaseous O_2 at appropriate temperature and oxygen partial pressure (Galinsky et al., 2015; Gayán et al., 2012). Perovskite-based OCs were employed in chemical looping methane reforming processes (He and Li, 2015; Neal et al., 2014). Recently, nano-materials were adopted in the synthesis of OCs, aiming to inhibit the interaction between active compounds and inert supports, so as to achieve robust and regenerable OC reactivity (Tian et al., 2017a; Xu et al., 2015). Experiments have been carried out in thermogravimetric analyzers (TGA), batch fluidized bed reactors and pilot-scale CLC reactors to investigate the OC performance and to optimize operational condition. The development of OC materials lays the foundation for the industrial application of CLC technology.

Except for the development of promising OCs, another key issue for CLC is the design and operation of the chemical looping combustor. To date, several pilot-scale reactors, ranging from 1 kW_{th} to 1 MW_{th}, have been successfully operated in Europe (Abad et al., 2015; Kolbitsch et al., 2009; Markström et al., 2013; Penthor et al., 2015; Ströhle et al., 2014), Asia (Bao et al., 2013a; Ryu et al., 2005; Shen et al., 2010; Xiao et al., 2012) and U.S. (Siriwardane et al., 2016; Kim et al., 2013). Generally, there are two fluidized bed reactors in the CLC system, acting as air

* Corresponding author.
E-mail address: hzhao@hust.edu.cn (H. Zhao).

https://doi.org/10.1016/j.ijggc.2018.05.002
Received 15 September 2017; Received in revised form 25 April 2018; Accepted 1 May 2018
1750-5836/ © 2018 Elsevier Ltd. All rights reserved.

reactor and fuel reactor. The gas sealing between the two reactors is realized by non-mechanical loop seals (Berguerand and Lyngfelt, 2008b) or solid valves (Kim et al., 2013). A cyclone is adopted for solid and gas separation. Conversion of pyrolysis and gasification products of coal occurs in FR by the help of OC. Therefore, the solid residence time and solid-gas contact in the FR can significantly affect the fuel conversion efficiency. To achieve good CLC performance, the FR was operated in different fluidizing regimes to match different OCs and fuel types (Cuadrat et al., 2011; Kim et al., 2013; Kolbitsch et al., 2010; Markström et al., 2013). The idea of operating the FR in the bubbling fluidized regime was first put forward by Lyngfelt et al. (2001) and then several CLC systems were configured to enhance the solid residence time whilst maintaining sufficient bed inventory (Berguerand and Lyngfelt, 2008a), resulting in over 98% of carbon capture efficiency. Shen et al. (2010) utilized a spouted fluidized bed as FR to achieve well-mixed between gas and solid phases. The CO_2 capture efficiency was up to 95% when using NiO/Al_2O_3 as OC. For other CLC units, relatively high gas velocity was chosen to achieve high solid circulation rate, *e.g.*, operated in turbulent fluidizing regime (Kolbitsch et al., 2010). Although a high solid circulation rate could be achieved by increasing the gas velocity, the bed inventory and solid residence time would be limited to some extent in the meantime, so as to result in much lower CH_4 conversion. Generally, the char gasification process is the rate-limiting step in coal-derived CLC processes. To address this issue, Kim et al. (2013) used a moving bed as FR. Due to the sufficient contact between reducing gas and OC, the combustion efficiency was close to 100%. Besides, Markström et al. (2013) and Abad et al. (2015) designed a circulating fluidized bed as FR, using coal as fuel. The residual char could be further converted by recirculating to the FR together with a part of OCs. In this way, nearly 100% CO_2 capture efficiency was attained (Pérez-Vega et al., 2016).

Another important configuration of the CLC system is the carbon stripper, which is located along the route of OC from the FR to the AR. The carbon stripper generally consists of several interconnected chambers to increase the pathway of char and OC, and steam is usually introduced as gasification agent to accelerate coal char conversion. Berguerand and Lyngfelt (2008b) first designed a carbon stripper with two reaction chambers in a 10 kW_{th} CLC reactor for coal, and the CO_2 capture efficiency achieved was in the range of 82%–96%. Based on the experimental results of this CLC prototype, Markström et al. (2013) came up with a carbon stripper with four chambers and a common outlet configured at the top to recycle the flue gas of FR and un-combusted char back to the FR. Eventually, the CO_2 capture efficiency increased to 99%. Abad et al. (2015) designed a 50 kW_{th} CLC reactor for solid fuels with nearly the same configuration of carbon stripper as that of the 100 kW_{th} reactor in Chalmers. To meet the requirement of high solid circulation rate, several groups have adopted a circulation riser (pneumatic transport) (Berguerand and Lyngfelt, 2008a) or screw conveyor (Ströhle et al., 2014). In the *C.S.I.C.* research group, an interconnected fluidized bed was used as FR in a 50 kW_{th} *i*G-CLC (*in-situ* gasification CLC)/CLOU unit (Abad et al., 2015), which formed an independent solid circulation in the FR by using a dual loop seal. The CO_2 capture efficiency was 88% at its first run.

After the construction of a CLC system, well-organized tests should be carried out to investigate the effects of different operational parameters on its CLC performance. Firstly, the temperature of FR was recognized as one of the most significant factors. Generally, a higher temperature in the FR showed a positive effect on the CLC performance because both the reactivity of OC and the gasification rate of coal could be enhanced at higher temperature (Cuadrat et al., 2011). However, sintering issue was found to occur to Ni-based OC when the temperature of FR was over 960 °C (Shen et al., 2009). Secondly, a larger amount of OC inventory in FR could provide more lattice oxygen for fuel conversion, so as to increase the CO_2 capture efficiency and the combustion efficiency (Linderholm et al., 2014). Thirdly, the decrease of superficial gas velocity in the FR could increase the residence time of the volatile matters and gasification products of char, within the same fluidizing regime. Thus, the CO_2 yield and carbon capture efficiency could be promoted (Cuadrat et al., 2012). Fourthly, the solid circulation rate is also a crucial influencing factor. Generally, the solid circulation rate should be in a reasonable range: on the one hand, the solid circulation rate should be high enough to provide sufficient lattice oxygen needed for fuel conversion; on the other hand, residual char can be transported into the AR at typical high solid circulation rate, thus decreasing the carbon capture efficiency (Shen et al., 2010). In addition, other factors, such as coal feeding rate and the gas velocity in carbon stripper, were also found to influence the CLC performance (Mendiara et al., 2013; Pérez-Vega et al., 2016). Linderholm et al. (2012) investigated the CLC performance by varying the locations of coal feeding spot, and found that the in-bed feed could improve the gas conversion by enhancing the contact between the oxygen carrier and volatile gases produced in the fuel chute. As reviewed above, the operational condition of CLC unit should be systematically investigated for better understanding of the characteristics of reactors and to optimize the operational parameters.

Development of CLC in Huazhong University of Science and Technology has been conducted in four steps. The first step was the selection and optimization of OC in TGA and batch fluidized bed reactor. In this step, most characteristic parameters, such as bed inventory, oxygen to fuel ratio, reaction temperature, solid circulation rate and reaction kinetics, were determined (Ma et al., 2017; Mei et al., 2013; Su et al., 2017a,b; Tian et al., 2017b; Tian et al., 2015; Wang et al., 2015; Yang et al., 2014a; Yang et al., 2014b; Zhao et al., 2014), which provide critical basic knowledge for the design of large-scale CLC reactor. The next step was to construct the cold-flow model reactor based on the geometric dimension of the hot reactor and the scaling rules. The hydrodynamic performance of the cold-flow model was investigated (Ma et al., 2012). In the process of designing a CLC reactor, a lab-scale continuously-operated reactor was important to demonstrate the manoeuvrability of the reactor, known as the third step. In this step, efforts were focused on the stability and flowability of OC particles, the operation conditions of different components (loop seal, cyclone, *etc.*), the associated operation parameters in the FR (such as OC to fuel ratio, superficial gas velocity, bed inventory and solid circulation rate, *etc.*) (Ma et al., 2015a; Ma et al., 2015b). Thus, the design and operation of the pilot-scale CLC system was optimized before the scale-up. A dual circulating fluidized bed design was chosen for the 5 kW_{th} lab-scale CLC reactor. When scaling up to the 50 kW_{th} pilot-scale CLC reactor, a similar dual circulating fluidized bed design was adopted. Furthermore, the combined unit of carbon stripper and loop seal was also introduced. The 50 kW_{th} reactor was built and operated to better understand the OC cycling behaviour and to gain valuable operation experience. All these works can lay the basis for the fourth step, *i.e.*, scaling-up of the reactor for industrial application. During these steps, CFD modelling was also conducted, which was helpful for the understanding of the hydrodynamics, heat and mass transfer as well as solid circulation behaviour between the two reactors (Su et al., 2015). All these will finally promote the innovation of CLC technology.

The objective of this work is to investigate the performance of the newly constructed 50 kW_{th} CLC reactor under different operation conditions. Low-cost and environmentally friendly hematite was selected as OC. The operational parameters, such as temperature, superficial gas velocity, fluidization gas composition and bed inventory in fuel reactor, were investigated during the continuous experiments.

2. Experimental

2.1. Introduction to the 50 kW_{th} CLC reactor

A 50 kW_{th} *in-situ* gasification chemical looping combustion (*i*G-CLC) reactor for coal was designed and constructed. The system is mainly consisted of air reactor, fuel reactor, loop seal (LS), carbon stripper

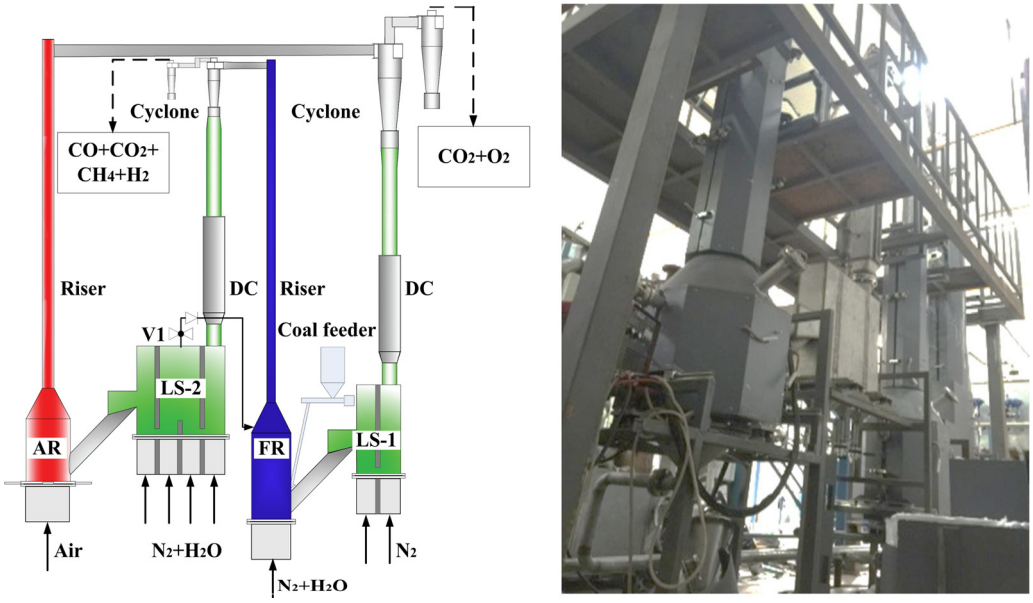

Fig. 1. Schematic view and a picture of the 50 kW_{th} *i*G-CLC reactor.

Table 1
Design parameters of the *i*G-CLC reactor.

	AR/Riser	FR/Riser	LS + CS
Diameter (m)	0.40/0.10	0.35/0.06	0.20 × 0.80 in rectangle
Height (m)	0.55/3.37	0.75/3.20	0.80
U_g (m/s)	0.59/8.19	0.3/7.08	0.03–0.15
Bed inventory (kg)	75	100	150
Operation temperature (°C)	900–1000	900–1000	900–1000
Fluidizing agent	air	50 vol.% H_2O + 50 vol.% N_2	50 vol.% H_2O + 50 vol.% N_2

(CS), cyclone and down comer (DC), as shown in Fig. 1.

Air reactor: The air reactor was operated in the turbulent fluidizing regime (0.5 U_t for air, here U_t is the terminal velocity of the OC), where homogeneous gas-solid phases distribution and relatively small pressure fluctuation was achieved.

Fuel reactor: The fuel reactor was operated as a bubbling fluidized bed (15 U_{mf}, where U_{mf} is the minimum fluidization velocity of the OC). A gas mixture of steam and N_2 was used as fluidizing agent. The OC inventory was 100 kg in the FR, corresponding to 2000 kg/MW_{th} for this kind of hematite OC.

Riser: Risers were designed to provide the driving force for OC circulation, usually operated at the fast fluidizing regime. The superficial gas velocity increased to 8.19 m/s by decreasing of the cross-sectional area. Moreover, the solid circulation in the FR and AR was controlled independently, as shown in Fig. 1.

Loop seal: LS-2 was designed as a four-chamber reactor, acting as loop seal and carbon stripper as well. The first chamber was operated at the moving bed regime to balance the pressure difference between the two reactors. The second and third chambers were fluidized by steam to gasify the unconverted char particles entrained by the OC. At the top of second and third chambers, the gases (with combustible species contained) were recycled to the FR for further conversion, so as to improve the carbon capture efficiency. The fourth chamber was designed to transport the reduced OC to AR for regeneration. LS-1 with two chambers was designed based on the regular design criteria.

Down comer: Different from the conventional circulating fluidized bed, a much higher solid circulation rate is required in a CLC reactor. Thus, a relatively large cross-sectional area of down comer is designed. Furthermore, three visual windows were installed in the middle of the down comer along the y-axis to monitor the operation status of solid circulation.

Cyclone: Two series-wound cyclones were used for solid-gas separation: the first cyclone was used for the separation of OC and the second one was for the separation of coal ash.

The auxiliary components were the coal screw feeder, gas supplying unit and preheating unit, off-gas treatment unit and online gas analysing unit. The coal feeding duct is 60 mm in diameter and the coal feeding point is located at 150 mm above the distributer, which is within the dense-phase zone, in order to achieve a high residence time and good contact with OC. High-pressure nitrogen was supplied to flush the coal into the bubbling fluidized bed fuel reactor. The off-gas treatment unit included a water-cooler jacket and a particulate matters filter. The off-gas of the FR and AR were analysed by two separated online gas analyzers.

The design parameters of the 50 kW_{th} reactor are listed in Table 1. Based on the fluidization regime map provided by Bi and Grace (1995), the superficial gas velocity in the AR was 0.5 U_t (U_t = 1.17 m/s at 950 °C for air) and the superficial gas velocity in the FR was 15 U_{mf} (U_{mf} = 0.02 m/s at 950 °C using 50 vol.% H_2O + 50 vol.% N_2 as fluidizing agent), while it was 8.19 m/s (7 U_t) in the riser (AR side). Note that, these characteristic velocities were calculated based on the average diameter of the OC. The reactor system was separately heated by electric furnaces.

2.2. Oxygen carrier and coal

The chemical analysis of hematite is shown in Table 2, as determined by the X-ray fluorescence (XRF, EDAX EAGLE III) and X-ray diffraction (XRD, X'Pert PRO) analysis. According to the experimental results of the various hematite that have been investigated in our batch fluidized bed reactor and 5 kW_{th} interconnect fluidized bed reactor, most of the hematite samples showed a promising reactivity and sufficient fluidization ability, with the active phase of Fe_2O_3 ranged from

Table 2
Chemical analysis of the hematite.

Composition	Fe_2O_3	SiO_2	CaO	Others
wt.%	90.09	3.41	5.33	1.17

Table 3
Proximate and ultimate analyses of Shenhua bituminous coal.

Solid fuel	Proximate (wt.%, ad)				Ultimate (wt.%, ad)				
	Moisture	Volatiles	Ash	Fixed carbon	C	H	N	S	O
Shenhua coal	1.66	15.54	34.34	48.46	55.26	2.12	0.79	0.44	5.39

65.9 wt.% to 91.65 wt.% (Ma et al., 2017) (Ma et al., 2015b) (Ma et al., 2015a) (Yang et al., 2014b). Hence, a batch of 500 kg hematite was purchased from the same origin place as the hematite (Fe_2O_3 was around 90 wt.%) from Australia (Ma et al., 2017) for the operation of the 50 kW_{th} reactor. The hematite was sieved in range of 150–350 μm, with an average diameter of 247 μm, measured by laser particle size analyzer (Malvern, Master Min). The true density of the OC particles was 3650 kg/m^3, measured by density analyzer (Micromeritics, AccuPyc1330). The crushing strength was 2.83 ± 0.2 N (the average value of 20 measurements), as determined by a digital dynamometer (Shimpo, FGP-100).

Shenhua bituminous coal from China was used as fuel in this work. The proximate and ultimate analyses are presented in Table 3. The coal was sieved to the diameter range of 100–300 μm.

2.3. Operational condition

Table 4 shows the operational conditions during the continuous experiments. Air was introduced into the AR at a constant velocity of 0.5 U_t. The loop seal and carbon stripper were fluidized by 50 vol.% H_2O + 50 vol.% N_2, where steam also acted as the gasification agent.

The effects of different operational parameters on the *i*G-CLC performance were investigated. Both No.2 and No.3 cases lasted for 120 min, while the other cases lasted for 60 min. Cases No.1, No.2 and No.3 were set to investigate the effect of FR temperature, which ranged from 900 °C to 1000 °C. The effect of inlet gas velocity was studied by experiments No.1, No.4 and No.5. Moreover, tests No.1, No.6 and No.7 were operated at different H_2O concentrations in the fluidizing gas. To be noted, due to the significant impact of temperature on the *i*G-CLC performance, the investigation of other operational parameters was conducted at relatively low temperature, *i.e.*, 900 °C, and thereby the differences could be distinguished.

2.4. Data evaluation

The gas species at the outlet of the FR mainly include CH_4, H_2, CO and CO_2. The oxygen demand (Ω_{OD}) is calculated as,

$$\Omega_{OD} = \left(0.5\chi_{CO} + 2\chi_{CH_4} + 0.5\chi_{H_2}\right)/\left(\Phi_0\left(\chi_{CO} + \chi_{CH_4} + \chi_{CO_2}\right)\right) \quad (1)$$

Thus, the combustion efficiency (η_{comb}) is defined as,

$$\eta_{comb} = 1 - \Omega_{OD} \quad (2)$$

where, χ_{CO}, χ_{CH_4}, $\chi_{H_2}$and χ_{CO_2} are the volume fraction of CO, CH_4, H_2 and CO_2 at the outlet of FR, respectively; Φ_0 is the ratio of moles of oxygen needed to completely convert per mole of carbon in the fuel (Markström et al., 2013).

Table 4
Operational condition of tests in the 50 kW_{th} *i*G-CLC reactor.

Operational condition	U_{FR}/U_{mf}	Operational temperature (ST_{FR}), °C	H_2O ratio (R_{H2O}), vol.%
No.1	15	900	50
No.2	15	950	50
No.3	15	1000	50
No.4	10	900	50
No.5	20	900	50
No.6	15	900	25
No.7	15	900	75

The carbon capture efficiency is defined as the ratio of carbon containing gas flow leaving the FR to the total carbon containing gas flow leaving the unit,

$$\eta_{CC} = \left(F_{CO_2,FR} + F_{CO,FR} + F_{CH_4,FR}\right)/\left(F_{CO_2,AR} + F_{CO_2,FR} + F_{CO,FR} + F_{CH_4,FR}\right) \quad (3)$$

here, $F_{CO_2,FR}$, $F_{CO,FR}$ and $F_{CH_4,FR}$ are the molar flow rates of CO_2, CO and CH_4 at the outlet of FR, respectively, calculated based on N_2 balance. $F_{CO_2,AR}$ is the molar flow rate of CO_2 at the outlet of AR.

The CO_2 yield (γ_{CO_2}), which presents the fraction of CO_2 in total gaseous carbon species leaving the FR, is defined by,

$$\gamma_{CO_2} = \chi_{CO_2}/\left(\chi_{CO} + \chi_{CH_4} + \chi_{CO_2}\right) \quad (4)$$

During the *i*G-CLC process, coal devolatilization and char gasification are the initial steps in the FR, as Eqs. (R3)–(R6). Because of the high oxygen to fuel ratio in the test, the active component (Fe_2O_3) in OC is only reduced to Fe_3O_4. The reactions between combustible gases and OC are shown in R7-R9. The water gas shift reaction and steam methane reforming reaction are shown as R10 and R11, respectively.

$$\text{Coal} \rightarrow \text{Char+Volatile+H}_2\text{O+Ash} \quad (R3)$$

$$\text{Volatile} \rightarrow \text{n}_1\text{CO}_2\text{+n}_2\text{CO+n}_3\text{CH}_4\text{+n}_4\text{H}_2\text{+n}_5\text{H}_2\text{O} \quad (R4)$$

$$\text{C+H}_2\text{ O= CO+H}_2 \quad (R5)$$

$$\text{C+CO}_2 = 2\text{CO} \quad (R6)$$

$$\text{CH}_4\text{+12Fe}_2\text{O}_3 = 8\text{Fe}_3\text{O}_4\text{+H}_2\text{O+CO}_2 \quad (R7)$$

$$\text{CO+3Fe}_2\text{O}_3 = 2\text{Fe}_3\text{O}_4\text{+CO}_2 \quad (R8)$$

$$\text{H}_2\text{+3Fe}_2\text{O}_3 = 2\text{Fe}_3\text{O}_4\text{+H}_2\text{O} \quad (R9)$$

$$\text{CO + H}_2\text{ O= CO}_2\text{+H}_2 \quad (R10)$$

$$\text{CH}_4\text{ + H}_2\text{ O= CO+3H}_2 \quad (R11)$$

3. Results

3.1. System behaviour and overall performance

Continuous tests were achieved at different temperatures, with relatively stable pressure drop and temperature in FR during the operation, as shown in Fig. 2. Correspondingly, the outlet gases concentrations of AR and FR during the tests at different temperature were also measured, as shown in Fig. 3. The coal feeding rate was 7.3 kg/h, corresponding to a nominal thermal power of 50 kW_{th}. Note that, the thermal power input was calculated on the basis of the lower heating value of Shenhua coal (24.8 MJ/kg). The other operational parameters were set at the basic condition as shown in Table 4. As illustrated in Fig. 2, the pressure drop of the FR ranged between 7.2 kPa and 7.7 kPa, indicating that the operation was relatively stable. The reduced amount of bed material is positively correlated to the decrease of the pressure drop in fuel reactor. The result showed that the pressure drop decreased by 0.25 kPa, which indicated that the decreased bed inventory of FR was approximately 3.3 kg. This was explained by the mass loss from the fuel reactor or the redistribution of the bed material in the whole reactor system. When the FR was operated at 900 °C, unconverted CO,

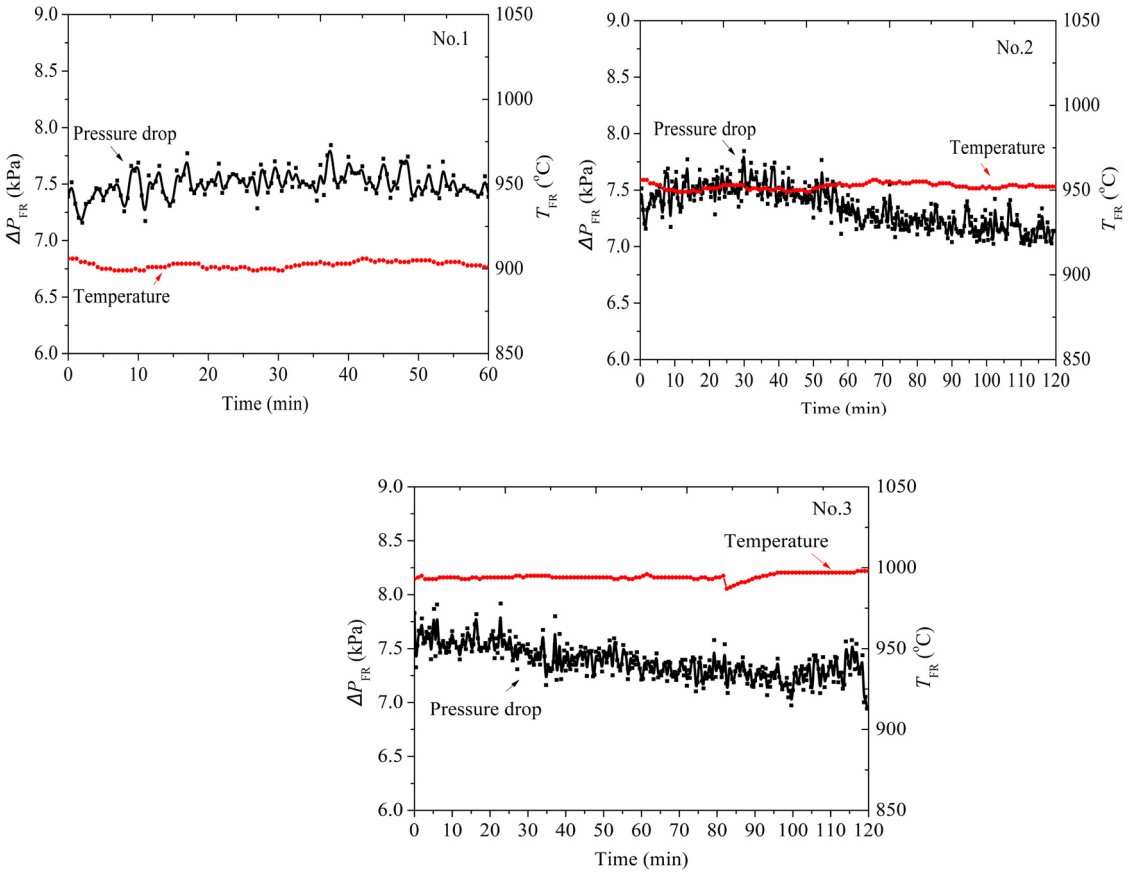

Fig. 2. Pressure drop and temperature of FR during tests No.1, No.2 and No.3.

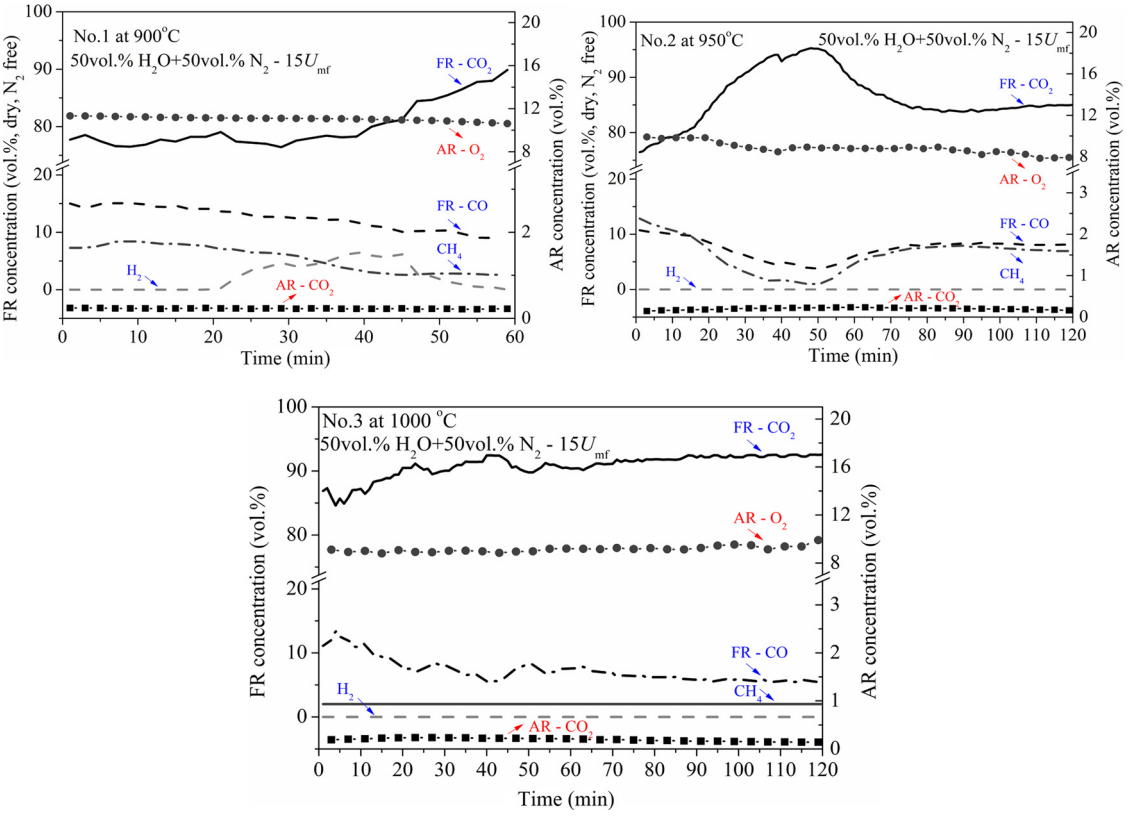

Fig. 3. Gas concentrations at the outlet of AR and FR at different temperatures (900 °C, 950 °C and 1000 °C).

CH_4 and H_2 were detected, as shown in Fig. 3. The coal screw feeder became slow after 40 min (resulting in the continuously decreasing of the coal feeding rate, which was probably caused by the unstable manner of the coal screw feeder or the block of the coal duct), leading to the increased concentration of CO_2 and decreased concentrations of CO, CH_4 and H_2. To be more specific, the gases concentration in the FR were 77 vol.% CO_2, 14 vol.% CO, 7 vol.% CH_4 and 2 vol.% H_2 in average. As known, CO could be generated by the coal pyrolysis and char gasification reactions, while CH_4 was mainly formed during the coal pyrolysis process. The escape of unconverted CO can be explained by the relatively low reactivity of hematite OC and the release of uncombusted CH_4 was attributed to the insufficient contact between gas-solid phases in the bubbling fluidized bed. The unconverted H_2 could be generated from the char gasification with steam, as shown in R5. The gas concentration of the AR was 11 vol.% O_2 and 0.22 vol.% CO_2 (with the rest being N_2), indicating that very little residual char was transported to the AR.

The average volume fraction of CO_2 from the FR outlet increased to 86 vol.% at 950 °C, while the H_2 concentration decreased to zero (also the case for the test at 1000 °C). This result can be explained by the high reactivity of H_2 towards hematite OC and fast reaction rate of char gasification (R5). However, there was still 6 vol.% of CH_4 in the exhaust of FR, which was almost equal to that at 900 °C. The main explanation was that the CH_4 was rapidly released during the coal pyrolysis process and escaped from the reactor without sufficient contact with OC. The CO concentration decreased to 8 vol.% at 950 °C, due to the improved reactivity of hematite and char gasification rate at high temperature. Thus, less residual char was transported to AR with OC circulation, as confirmed by the small fraction of CO_2 from the outlet of AR (the gas concentration of AR was decreased to 8.7 vol.% O_2 and 0.20 vol.% CO_2 (with the rest being N_2). The result showed that the residual char being transported to AR reduced with the increased Fuel reactor temperature). When the temperature of the FR increased to 1000 °C, the gas concentration of the FR was 91 vol.% CO_2, 7 vol.% CO, 2 vol.% CH_4 and 0 vol.% H_2, and the O_2 and CO_2 concentrations of the AR outlet decreased to 8.2 vol.% and 0.15 vol.%, respectively.

In the *i*G-CLC process, there are two ways to generate combustible gases (Adanez et al., 2012): the coal pyrolysis (CH_4, CO and H_2) and the char gasification (CO and H_2). The extent of CH_4 conversion could be an index of reaction between volatile and hematite OC, because CH_4 was assumed to only generate from coal pyrolysis process (Pérez-Vega et al., 2016). The conversion of CH_4 was almost unchanged when the operation temperature increased from 900 °C to 950 °C, even though the reactivity of OC was theoretically higher at 950 °C. This result indicated that the sufficient contact between volatile and OC was a crucial factor for *i*G-CLC reactor.

With the increase of the FR temperature, the char gasification rate accelerated and the reactivity of OC was also promoted. In this sense, the residence time of char is a key issue to affect the char gasification extent. Note that the CO_2 percentage in the AR outlet showed a decreasing trend with the increase of temperature. This was explained by that more char was gasified at higher temperatures in the FR and thus a relatively small amount of char was transported to the AR. It was also found that more CO, CH_4 and H_2 was converted by OC at elevated temperature, contributing to a higher CO_2 yield.

3.2. Effect of FR temperature

Fig. 4 shows the average combustion efficiency (η_{Comb}), carbon capture efficiency (η_{CC}) and CO_2 yield (γ_{CO2}) values at different operating temperatures. The combustion efficiency was 0.70 at 900 °C and increased to 0.86 at 1000 °C. The results were almost in the same range of the oxygen demand as the 100 kW_{th} CLC combustor in Chalmers (the oxygen demand was 16% lower) (Markström et al., 2013), while it was higher than the oxygen demand of the 50 kW_{th} CLC combustor in *C.S.I.C.* (Abad et al., 2015). It could be explained by the well-mixing

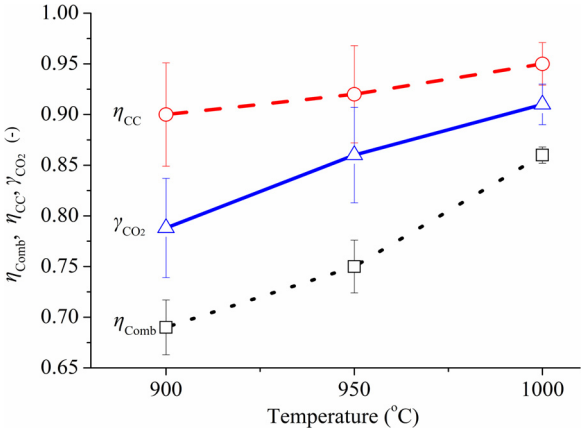

Fig. 4. Combustion efficiency (η_{Comb}), carbon capture efficiency (η_{CC}) and CO_2 yield (γ_{CO2}) at different temperatures in FR.

between the quick-released volatile products and OC in the relatively smaller cross-section of the FR in *C.S.I.C.* (Abad et al., 2015).

Clearly, the operational temperature in the FR had a great impact on the combustion efficiency because more generated combustible gases (CO, CH_4 and H_2) would be oxidized by OC at elevated temperature, due to the promoted reactivity of OC, which was also identified by Pérez-Vega at the continuously test in 50 kW_{th} CLC reactor in *C.S.I.C.*, using the ilmenite as OC and bituminous coal as fuel (Pérez-Vega et al., 2016). Note that at 1000 °C, the unconverted CH_4 sharply decreased, which contributed to the decrease of the oxygen demand. Obviously, higher temperature (such as 1000 °C) is beneficial for the conversion of CH_4 (main products of coal pyrolysis), which is mainly attributed to the reforming of CH_4. Generally, the amount of CO and H_2 from char gasification increased with temperature in the absence of OC. Here, in the CLC atmosphere, the volume fraction of CO dropped from 14 vol.% at 900 °C to 8 vol.% at 950 °C, and slightly decreased to 7 vol.% at 1000 °C. In this sense, to improve the combustion efficiency, we can increase the residence time of char or use more highly reactive OC, such as Cu-decorated hematite (Yang et al., 2014a), the mixture of hematite and copper ore (Yang et al., 2014b)/manganese (Linderholm et al., 2016).

The CO_2 yield is relevant to the reactivity of OC, the bed inventory and the residence time of combustible gases. The highest CO_2 yield was achieved at 1000 °C. When compared to the performance of the 1 kW_{th} CLC reactor (Song et al., 2013), the CO_2 yield of which was 0.76 at 950 °C, slightly higher CO_2 yield of 0.85 was attained in the present reactor. The explanation could be the higher bed inventory (corresponding to 2000 kg/MW_{th}) and also the higher height of FR to improve the residence time of combustible gases.

The carbon capture efficiency was always higher than 0.90 within the temperature range of 900–1000 °C. Generally, the carbon capture efficiency can be affected in two aspects: 1) the residual char being transported from the FR to the AR along with OC, and 2) the gas leakage between the AR and FR. For the experiments at different temperatures, the gas leakage should be equal. Thus, the carbon capture efficiency could only be affected by the unconverted char carried by OC from the FR to the AR. As the higher temperature was beneficial for coal char gasification, less residual char would be left without being converted in the FR, as well as less residual char being transported into the AR. Consequently, much higher carbon capture efficiency can be achieved at elevated temperature. This result suggested that the temperature of the FR should be as high as possible to achieve full char conversion (Pérez-Vega et al., 2016). With respect to the circulation of OC by the riser rather than the overflow (Song et al., 2013), more sufficient residence time of char in the FR would be attained, resulting in a higher carbon capture efficiency.

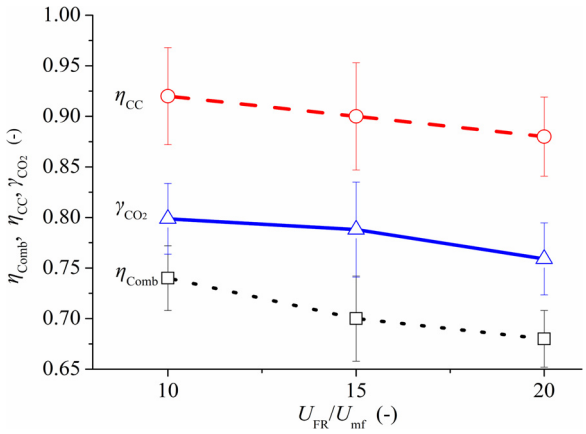

Fig. 5. Combustion efficiency, η_{Comb}, carbon capture efficiency, η_{CC}, and CO_2 yield, γ_{CO2}, *vs.* superficial gas velocity in FR, U_{FR}.

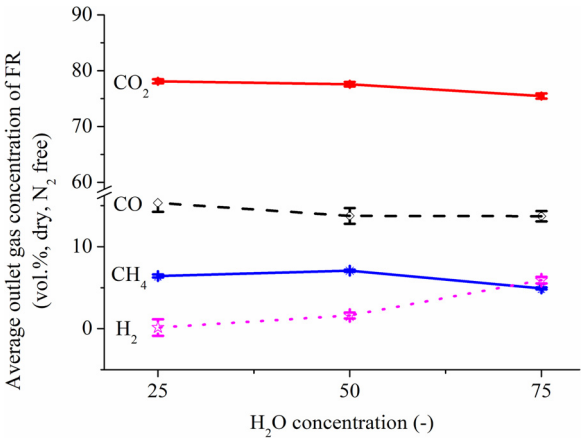

Fig. 6. Average outlet gas concentration of FR at different H_2O concentration.

3.3. Effect of inlet gas velocity in FR

The effect of inlet gas velocity in the FR (U_{FR}) on the combustion efficiency, carbon capture efficiency and CO_2 yield are shown in Fig. 5. These experiments were carried out at 900 °C with a bed inventory of 100 kg in the FR. The increase of inlet gas velocity in the FR showed a negative effect on the combustion efficiency, which was 0.74 at 10 U_{mf} and decreased to 0.68 at 20 U_{mf}. The carbon capture efficiency and CO_2 yield both decreased by about 0.04 from 10 U_{mf} to 20 U_{mf}. This can be explained by the decreased residence time of the volatiles and a lower bed inventory (due to the increased gas volume fraction) in the FR at elevated inlet gas velocity. Thus, the conversion of the volatile and gasification products (CH_4, CO and H_2) should be improved due to more sufficient reaction time. However, the combustion efficiencies were relatively lower than other results (Pérez-Vega et al., 2016), which was attributed to the only partially oxidized gas-phase products. It could be addressed by achieving better contact between the gas-solid phases or using a more reactive OC.

The CO_2 yield only varied in a narrow range of 0.77-0.80 because of the excess of bed inventory in the FR. Thus, the oxidization of CO/CH_4/H_2 to CO_2/H_2O was easily achieved by the help of sufficient lattice oxygen under the different superficial gas velocity in the FR (10–20 U_{mf}). The oxidization of CH_4 by hematite was controlled by the chemical reaction rate and the unconverted CH_4 was due to the limited hematite reactivity (Ma et al., 2015b). Therefore, the operational temperature of FR can affect more on the CO_2 yield than the inlet gas velocity in FR when the bed inventory is abundant. However, it should be noted that the generated gases (mainly CO_2 and H_2O) of coal pyrolysis and char gasification products also acted as fluidizing agent. If assumed that the coal was all converted to gases and thereby the generated gases reduce the ratio of effective fluidizing velocity from a ratio of 2:1 (between 20 and 10 U_{FR}/U_{mf}) to 1.7:1. Thus, the changes in the inlet gas velocity (from 10 U_{mf} to 20 U_{mf}) could pose relatively weak effect on the residence time of char. However, the CLC performance (η_{Comb}, η_{CC} and γ_{CO2},) was still impacted by the inlet gas velocity in FR.

With respect to the carbon capture efficiency, the results showed that the unconverted gasification products (CO and H_2) were increased at higher inlet gas velocity in FR, which was in line with the prediction of the carbon capture efficiency by Markström et al. (2010): the carbon capture efficiency could promote at the longer residence time. In this work, the carbon capture efficiency only decreased by 0.05 from 10 U_{mf} to 20 U_{mf}. It was explained by the good performance of the carbon stripper, which reduced the effect of the inlet gas velocity in the FR on the carbon capture efficiency. Nevertheless, the performance of carbon stripper should be investigated in detail in future work.

3.4. Effect of H_2O concentration

To evaluate the effect of H_2O concentration on the CLC performance, the H_2O concentration of inlet gas was varied in the range of 25 vol.%–75 vol.%. The other operational parameters were 900 °C, 15 U_{mf} and 100 kg OC inventory in the FR. It should be noted that H_2O in fluidizing gas acted as both gasification agent and fluidization agent. The presence of steam could promote the char gasification reaction (R5) and water gas shift reaction (R10). The average outlet gas composition of the FR at different H_2O concentrations is shown in Fig. 6. The CO_2 fraction increased from 75 vol.% to 80 vol.% when the H_2O concentration varied from 25 vol.% to 75 vol.%. Moreover, at 75% H_2O concentration, the unconverted CH_4 decreased to 5 vol.% and the H_2 concentration became as high as 6 vol.%, because the steam methane reaction (SMR) was significant at 900 °C, to consume CH_4 and generate H_2. The CO concentration was theoretically raised at the evaluated H_2O concentration if without the presence of OC. However, the experimental result of CO fraction was almost steady because the relatively high reaction rate of CO and H_2 with the OC (Cuadrat et al., 2012)

The combustion efficiency, carbon capture efficiency and CO_2 yield at different H_2O concentrations in inlet gas are shown in Fig. 7. The carbon capture efficiency was relatively stable at different H_2O concentrations (all above 0.9), which can be explained by the sufficient solid residence time in the FR to gasify the char and the reliable performance of carbon stripper to reduce the residual char. The CO_2 yield improved from 0.76 at 25 vol.% H_2O concentration to 0.81 at 75 vol.% H_2O concentration, because more CH_4 was reformed by steam and then the SMR products (CO and H_2) were oxidated by OC to CO_2 and H_2O, as

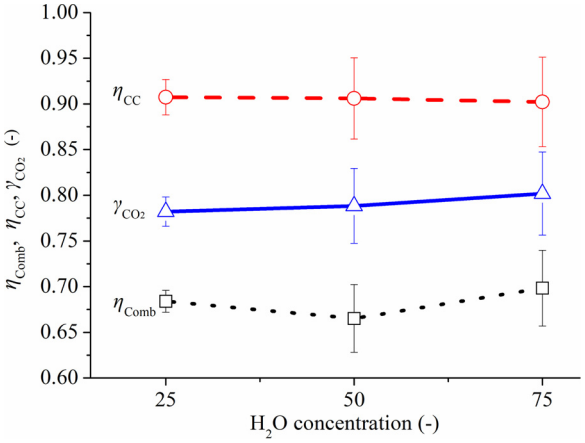

Fig. 7. Combustion efficiency (η_{Comb}), carbon capture efficiency (η_{CC}) and CO_2 yield (γ_{CO2}) at different H_2O concentrations in inlet gas.

shown in Fig. 6. The lowest combustion efficiency was attained at 50 vol.% H_2O, due to the relatively high CH_4 fraction. The highest combustion efficiency of 0.7 was achieved at 75 vol.% H_2O.

4. Discussion

4.1. Geometric dimension

The circulating fluidized bed reactor is a suitable choice for CLC technology, as demonstrated by Berguerand and Lyngfelt (2008a), Abad et al. (2015), Ströhle et al. (2014). Whereas, the geometric dimensions of reactor are determined by many factors, such as the choice of the fluidized regime, types of OC and coal, the circulating configuration, *etc*.

Note that, if we scale up to a 500 MW_{th} power plant on the basis of the current reactor design, the cross-sectional areas would be quite large due to the relatively low gas velocity in AR and FR. For the 50 kW_{th} lab-scaled reactor, the height of the reactor was limited by the height of the room, which would lead to very short solid residence time at high gas flow rates. Whereas, for the actual CLC power plant, higher residence time could be achieved due to the enough space for the reactor. Thus, the superficial gas velocity in air reactor and fuel reactor is located in the same regime as the circulating fluidized bed, which was suggested to be 7.3 m/s in AR and 5.2 m/s in FR, respectively by Lyngfelt and Bo (2015). In this way, the cross-sectional area of AR and FR would significantly decrease. Based on the design criterion, the mass flow rate of air is calculated according to the air ratio and the oxygen demand, and the cross-sectional area can be calculated from the designed air mass flow rate and superficial gas velocity. If the 7.3 m/s is designed as the gas velocity in AR and 5.2 m/s in FR, the diameter of AR and FR would be 11 m and 8 m, respectively. This geometric dimension will be reasonable.

4.2. Operational parameters

The velocity in the carbon stripper is lower than that of previous works (Pérez-Vega et al., 2016). To be honest, we did not lay much emphasis on the study of the CS at the initial run, but mainly focused on the goal of successful and continuous operation. The reason for choosing the operational fluidization regime was demonstrated as below:

1) The down comer connected to the cyclone of FR was operated as a moving bed, which could provide sufficient residence time for the residual char (entrained with OC) gasification by steam in the fluidizing gas in the first chamber, and then the gasification products could be further oxidized by the OC in the down comer and first chamber in the CS + LS, where 150 kg of hematite OC was loaded (higher than the 100 kg bed inventory in FR). The well-mixing of the gasification products and OC was realized by the reversal gas-solid flow, which could enhance the conversion of fuel. This configuration is similar to the design of FR at Ohio State University (Kim et al., 2013).
2) The second and third chambers acted as carbon strippers, they were operated at the bubbling bed regime at the initial experiment. For the escaped residual char from the first chamber, it will also be gasified by steam and then converted to CO_2 and H_2O. At the first run of the reactor, both the operational parameters and the reactor system should be simple enough to achieve a quick stable condition, which include the system pressure balance, solid circulation establishment, stable operational temperature and good performance of cyclone, *etc*. Thus, the duct for transferring the gasification products or the residual char was switched off in order to minimize the effect of pressure fluctuation in FR on the stable operation of the loop seal and carbon stripper. The gas velocity decreased as the gas velocity in the carbon stripper was located in the manageable bubbling fluidization regime and then higher residence time could be attained. Furthermore, the function of the carbon stripper as a particle separator in the 50 kW_{th} reactor system was compromised currently, where the gasification products of carbon residue within carbon stripper might pass through the downcomer and then to the FR cyclone, leading to the reduced combustion efficiency, or through the air reactor, resulting in the reduced carbon capture efficiency. Further work should be conducted to investigate the enhanced performance of the carbon stripper comprehensively.

5. Conclusion

A 50 kW_{th} interconnected fluidized bed reactor for *i*G-CLC of coal was designed, constructed and operated in this work. Natural hematite was used as oxygen carrier and Shenhua bituminous coal was used as fuel. The air reactor was operated at turbulent fluidizing regime while the fuel reactor was operated at bubbling fluidizing regime. A loop seal was designed for gas sealing and also played the role of carbon stripper, which was beneficial for enhancing solid fuel conversion. Two risers were adopted to provide the driving force for OC circulation in the FR and AR independently. Tests under different operational parameters were conducted to evaluate the performance of the *i*G-CLC reactor. The conclusions were drawn as follows:

(1) The highest combustion efficiency, carbon capture efficiency and CO_2 yield were 0.86, 0.95 and 0.91, respectively, at 1000 °C.
(2) Higher temperature promotes the reactivity of the hematite OC, resulting in complete conversion of H_2 and decreasing the amount of unconverted CH_4. Moreover, the entrained residual char was reduced and the CO_2 yield was improved, so as to lead to an increased carbon capture efficiency.
(3) Varying the inlet gas velocity in the range of 10–20 U_{mf} showed a significant impact on combustion efficiency.
(4) The H_2O concentration in inlet gas could affect the fraction of H_2 and CH_4 in the outlet gas of the FR at 900 °C, due to the CH_4 reforming reaction. CH_4 reforming reaction could result in the generation of CO and H_2, which are more reactive (with hematite) than that of CH_4. Thus, the combustion efficiency would be enhanced.

Acknowledgements

This work was presented and benefited from discussions at the “4th International Conference on Chemical Looping” (Nanjing, China, 2016). The authors acknowledge the support from the “National Key R &D Program of China (2016YFB0600801)” and “National Natural Science Foundation of China(51522603)”. The staff of the Analytical and Testing Center, Huazhong University of Science and Technology, are also appreciated for the related experimental analyses.

References

Abad, A., Pérez-Vega, R., de Diego, L.F., García-Labiano, F., Gayán, P., Adánez, J., 2015. Design and operation of a 50 kWth chemical looping combustion (CLC) unit for solid fuels. Appl. Energy 157, 295–303.
Adanez, J., Abad, A., Garcia-Labiano, F., Gayan, P., Diego, L.F.D., 2012. Progress in chemical-looping combustion and reforming technologies. Prog. Energy Combust. 38, 215–282.
Bao, J., Li, Z., Sun, H., Cai, N., 2013a. Continuous test of ilmenite-based oxygen carriers for chemical looping combustion in a dual fluidized bed reactor system. Ind. Eng. Chem. Res. 52, 14817–14827.
Bao, J., Li, Z., Sun, H., Cai, N., 2013b. Experiment and rate equation modeling of Fe oxidation kinetics in chemical looping combustion. Combust. Flame 160, 808–817.
Berguerand, N., Lyngfelt, A., 2008a. Design and operation of a 10 kWth chemical-looping combustor for solid fuels – testing with south african coal. Fuel 87, 2713–2726.
Berguerand, N., Lyngfelt, A., 2008b. The use of petroleum coke as fuel in a 10 kWth chemical-looping combustor. Int. J. Greenh. Gas Control 2, 169–179.
Bi, H., Grace, J., 1995. Flow regime diagrams for gas-solid fluidization and upward transport. Int. J. Multiphas Flow 21, 1229–1236.
Chevallier, J., 2010. Carbon capture and storage (CCS) technologies and economic investment opportunities in the UK. Glob. Bus. Econ. Rev. 12, 252–265.

Cuadrat, A., Abad, A., García-Labiano, F., Gayán, P., de Diego, L.F., Adánez, J., 2011. The use of ilmenite as oxygen-carrier in a 500Wth chemical-looping coal combustion unit. Int. J. Greenh. Gas Control 5, 1630–1642.
Cuadrat, A., Abad, A., García-Labiano, F., Gayán, P., de Diego, L.F., Adánez, J., 2012. Effect of operating conditions in Chemical-Looping Combustion of coal in a 500 Wth unit. Int. J. Greenh. Gas Control 6, 153–163.
Galinsky, N., Mishra, A., Zhang, J., Li, F., 2015. Ca1-xAxMnO3 (A = Sr and Ba) perovskite based oxygen carriers for chemical looping with oxygen uncoupling (CLOU). Appl. Energy 157, 358–367.
Gayán, P., Adánez-Rubio, I., Abad, A., Diego, L.F.D., García-Labiano, F., Adánez, J., 2012. Development of Cu-based oxygen carriers for chemical-looping with oxygen uncoupling (CLOU) process. Fuel 96, 226–238.
He, F., Li, F., 2015. Perovskite promoted iron oxide for hybrid water-splitting and syngas generation with exceptional conversion. Energ. Environ. Sci. 8, 535–539.
Ishida, M., Jin, H., 1994. A new advanced power-generation system using chemical-looping combustion. Energy 19, 415–422.
Kim, H., Wang, D., Zeng, L., Bayham, S., Tong, A., Chung, E., Kathe, M., Luo, S., McGiveron, O., Wang, A., Sun, Z., Chen, D., Fan, L., 2013. Coal direct chemical looping combustion process: design and operation of a 25-kWth sub-pilot unit. Fuel 108, 370–384.
Kolbitsch, P., Pröll, T., Bolhar-Nordenkampf, J., Hofbauer, H., 2009. Design of a chemical looping combustor using a dual circulating fluidized bed (DCFB) reactor system. Chem. Eng. Technol. 32, 398–403.
Kolbitsch, P., Bolhàr-Nordenkampf, J., Pröll, T., Hofbauer, H., 2010. Operating experience with chemical looping combustion in a 120 kW dual circulating fluidized bed (DCFB) unit. Int. J. Greenh. Gas Control 4, 180–185.
Leion, H., Mattisson, T., Lyngfelt, A., 2008. Solid fuels in chemical-looping combustion. Int. J. Greenh. Gas Control 2, 180–193.
Linderholm, C., Lyngfelt, A., Cuadrat, A., Jerndal, E., 2012. Chemical-looping combustion of solid fuels – operation in a 10 kW unit with two fuels, above-bed and in-bed fuel feed and two oxygen carriers, manganese ore and ilmenite. Fuel 102, 808–822.
Linderholm, C., Schmitz, M., Knutsson, P., Källén, M., Lyngfelt, A., 2014. Use of low-Volatile solid fuels in a 100 kW chemical-looping combustor. Energy Fuels 28, 5942–5952.
Linderholm, C., Schmitz, M., Knutsson, P., Lyngfelt, A., 2016. Chemical-looping combustion in a 100 kW unit using a mixture of ilmenite and manganese ore as oxygen carrier. Fuel 166, 533–542.
Lyngfelt, A., Bo, L., 2015. A 1000 MWth boiler for chemical-looping combustion of solid fuels – discussion of design and costs. Appl. Energy 157, 475–487.
Lyngfelt, A., Bo, L., Mattisson, T., 2001. A fluidized-bed combustion process with inherent CO2 separation; application of chemical-looping combustion. Chem. Eng. Sci. 56, 3101–3113.
Ma, J., Zhao, H., Mei, D., Lei, G., Zheng, C., 2012. Cold-flow model experiment of interconnected fluidized bed for chemical looping combustion of coal. Chin. J. Power Eng. 32, 909–915.
Ma, J., Zhao, H., Tian, X., Wei, Y., Rajendran, S., Zhang, Y., Bhattacharya, S., Zheng, C., 2015a. Chemical looping combustion of coal in a 5kWth interconnected fluidized bed reactor using hematite as oxygen carrier. Appl. Energy 157, 304–313.
Ma, J., Zhao, H., Tian, X., Wei, Y., Zhang, Y., Zheng, C., 2015b. Continuous operation of interconnected fluidized bed reactor for chemical looping combustion of CH4 using hematite as oxygen carrier. Energy Fuels 29, 3257–3267.
Ma, J., Tian, X., Zhao, H., Bhattacharya, S., Rajendran, S., Zheng, C., 2017. Investigation of Two hematites as oxygen carrier and two low-rank coals as fuel in chemical looping combustion. Energy Fuels 31, 1896–1903.
Markström, P., Berguerand, N., Lyngfelt, A., 2010. The application of a multistage-bed model for residence-time analysis in chemical-looping combustion of solid fuel. Chem. Eng. Sci. 65, 5055–5066.
Markström, P., Linderholm, C., Lyngfelt, A., 2013. Chemical-looping combustion of solid fuels – design and operation of a 100 kW unit with bituminous coal. Int. J. Greenh. Gas Control 15, 150–162.
Mattisson, T., 2013. Materials for chemical-looping with oxygen uncoupling. ISRN Chem. Eng. 2013.
Mei, D., Zhao, H., Ma, Z., Zheng, C., 2013. Using the Sol-gel-derived CuO/CuAl2O4 oxygen carrier in chemical looping with oxygen uncoupling for three typical coals. Energy Fuels 27, 2723–2731.
Mendiara, T., Diego, L., García-Labiano, F., Gayán, P., Abad, A., Adánez, J., 2013. Behaviour of a bauxite waste material as oxygen carrier in a 500 Wth CLC unit with coal. Int. J. Greenh. Gas Control 17, 170–182.
Neal, L., Shafiefarhood, A., Li, F., 2014. Dynamic methane partial oxidation using a fe2O3@La0.8Sr0.2FeO3-(core-shell redox catalyst in the absence of gaseous oxygen. ACS Catal. 4, 3560–3569.
Pérez-Vega, R., Abad, A., García-Labiano, F., Gayán, P., de Diego, L.F., Adánez, J., 2016. Coal combustion in a 50 kWth Chemical Looping Combustion unit: seeking operating conditions to maximize CO2 capture and combustion efficiency. Int. J. Greenh. Gas Control 50, 80–92.
Penthor, S., Zerobin, F., Mayer, K., Pröll, T., Hofbauer, H., 2015. Investigation of the performance of a copper based oxygen carrier for chemical looping combustion in a 120 kW pilot plant for gaseous fuels. Appl. Energy 145, 52–59.
Ryu, H., Jin, G., Yi, C., 2005. Demonstration of Inherent CO2 Separation and No NOx Emission in a 50 kW Chemical-Looping Combustor: Continuous Reduction and Oxidation Experiment, Greenhouse Gas Control Technologies 7. Elsevier Science Ltd, Oxford, pp. 1907–1910.
Shen, L., Wu, J., Gao, Z., Xiao, J., 2009. Reactivity deterioration of NiO/Al2O3 oxygen carrier for chemical looping combustion of coal in a 10 kWth reactor. Combust. Flame 156, 1377–1385.
Shen, L., Wu, J., Gao, Z., Xiao, J., 2010. Characterization of chemical looping combustion of coal in a 1kWth reactor with a nickel-based oxygen carrier. Combust. Flame 157, 934–942.
Siriwardane, R., Tian, H., Riley, J., Benincosa, W., Straub, D., Weber, J., Richards, R., 2016. Commercial scale preparations of CuO-Fe2O3-Alumina oxygen carrier with various techniques: bench scale fluidized bed tests with coal/air and methane/air and pilot scale (51 kWth) chemical looping combustion tests with methane/air. In: Proc. 4rd Int. Conf. on Chemical Looping. Nanjing, China.
Song, T., Shen, T., Shen, L., Xiao, J., Gu, H., Zhang, S., 2013. Evaluation of hematite oxygen carrier in chemical-looping combustion of coal. Fuel 104, 244–252.
Ströhle, J., Orth, M., Epple, B., 2014. Design and operation of a 1 MWth chemical looping plant. Appl. Energy 113, 1490–1495.
Su, M., Zhao, H., Ma, J., 2015. Computational fluid dynamics simulation for chemical looping combustion of coal in a dual circulation fluidized bed. Energ. Convers. Manage. 105, 1–12.
Su, M., Ma, J., Tian, X., Zhao, H., 2017a. Reduction kinetics of hematite as oxygen carrier in chemical looping combustion. Fuel Process. Technol. 155, 160–167.
Su, M., Zhao, H., Tian, X., Zhang, P., Du, B., Liu, Z., 2017b. Intrinsic reduction kinetics investigation on a hematite oxygen carrier by CO in chemical looping combustion. Energy Fuels 31.
Tian, X., Zhao, H., Wang, K., Ma, J., Zheng, C., 2015. Performance of cement decorated copper ore as oxygen carrier in chemical-looping with oxygen uncoupling. Int. J. Greenh. Gas Control 41, 210–218.
Tian, X., Wei, Y., Zhao, H., 2017a. Evaluation of a hierarchically-structured CuO@TiO2-Al2O3 oxygen carrier for chemical looping with oxygen uncoupling. Fuel 209, 402–410.
Tian, X., Zhao, H., Ma, J., 2017b. Cement bonded fine hematite and copper ore particles as oxygen carrier in chemical looping combustion. Appl. Energy 204, 242–253.
Wang, K., Zhao, H., Tian, X., Fang, Y., Ma, J., Zheng, C., 2015. Chemical-looping with oxygen uncoupling of different coals using copper ore as an oxygen carrier. Energy Fuels 29, 6625–6635.
Xiao, R., Chen, L., Saha, C., Zhang, S., Bhattacharya, S., 2012. Pressurized chemical-looping combustion of coal using an iron ore as oxygen carrier in a pilot-scale unit. Int. J. Greenh. Gas Control 10, 363–373.
Xu, Z., Zhao, H., Wei, Y., Zheng, C., 2015. Self-assembly template combustion synthesis of a core-shell CuO@TiO2-Al2O3 hierarchical structure as an oxygen carrier for the chemical-looping processes. Combust. Flame 162, 3030–3045.
Yang, W., Zhao, H., Ma, J., Mei, D., Zheng, C., 2014a. Copper-decorated hematite as an oxygen carrier for in situ gasification chemical looping combustion of coal. Energy Fuels 28, 3970–3981.
Yang, W., Zhao, H., Wang, K., Zheng, C., 2014b. Synergistic effects of mixtures of iron ores and copper ores as oxygen carriers in chemical-looping combustion. Proc. Combust. Inst. 35, 2811–2818.
Zhao, H., Wang, K., Fang, Y., Ma, J., Mei, D., Zheng, C., 2014. Characterization of natural copper ore as oxygen carrier in chemical-looping with oxygen uncoupling of anthracite. Int. J. Greenh. Gas Control 22, 154–164.